Plant Physiology Preview. Published on November 11, 2016, as DOI:10.1104/pp.16.00943

SHORT TITLE

cis-cinnamic acid is an auxin efflux inhibitor

CORRESPONDING AUTHORS

Bartel Vanholme
Department of Plant Systems Biology, VIB, B-9052 Gent, Belgium
Department of Plant Biotechnology and Bioinformatics, Ghent University, B-9052 Gent, Belgium
E-mail: bartel.vanholme@psb.vib-ugent.be
Telephone: + 32 (0)9 33 13 840

Wout Boerjan;
Department of Plant Systems Biology, VIB, B-9052 Gent, Belgium
Department of Plant Biotechnology and Bioinformatics, Ghent University, B-9052 Gent, Belgium
E-mail: wout.boerjan@psb.vib-ugent.be
Telephone: + 32 (0)9 33 13 881

ARTICLE TITLE

***cis*-cinnamic acid is a novel, natural auxin efflux inhibitor that promotes lateral root formation**

ALL AUTHORS NAME AND AFFILIATIONS

Ward Steenackers[1,2]
Petr Klíma[3]
Mussa Quareshy[4]
Igor Cesarino[1,2,5]
Robert P. Kumpf[1,2]
Sander Corneillie[1,2]
Pedro Araújo[1,2]
Tom Viaene[1,2],
Geert Goeminne[1,2]

Moritz K Nowack[1,2]
Karin Ljung[6]
Jiří Friml[7]
Joshua J Blakeslee[8]
Ondřej Novák[6,9]
Eva Zažímalová[3]
Richard Napier[4]
Wout Boerjan[1,2,†,*]
Bartel Vanholme[1,2,†,*]

[1]Department of Plant Systems Biology, VIB, B-9052 Gent, Belgium
[2]Department of Plant Biotechnology and Bioinformatics, Ghent University, B-9052 Gent, Belgium
[3]Institute of Experimental Botany, Czech Academy of Sciences, CZ-16502 Prague, Czech Republic
[4]School of Life Sciences, University of Warwick, Coventry CV4 7AL, United Kingdom
[5]Department of Botany, Institute of Biosciences, University of São Paulo, Butantã, São Paulo, Brazil
[6]Umeå Plant Science Centre, Department of Forest Genetics and Plant Physiology, Swedish University of Agricultural Sciences, SE-901 83 Umeå, Sweden
[7]Institute of Science and Technology, Austria (IST Austria), 3400 Klosterneuburg, Austria
[8]Department of Horticulture and Crop Science, the Ohio State University/OARDC, Wooster, OH 44691, USA
[9]Laboratory of Growth Regulators, Centre of the Region Haná for Biotechnological and Agricultural Research, Institute of Experimental Botany CAS and Faculty of Science of Palacký University, Šlechtitelů 27, CZ-78371 Olomouc, Czech Republic

†These authors contributed equally to this work and share last authorship.
*Corresponding authors. Bartel Vanholme; E-mail: bartel.vanholme@psb.vib-ugent.be; Telephone: + 32 (0)9 33 13 840. Wout Boerjan; E-mail: wout.boerjan@psb.vib-ugent.be; Telephone: + 32 (0)9 33 13 881.

ONE SENTENCE SUMMARY

The phenylpropanoid *cis*-cinnamic acid is natural auxin efflux inhibitor that promotes lateral root formation

LIST OF AUTHOR CONTRIBUTION

WS designed the experiments, performed most of the experiments, analyzed the data and wrote the article. PK performed the auxin accumulation assays. MQ performed auxin-binding

and anti-auxin experiments using Surface Plasmon Resonance (SPR), and did docking-analysis. IC assisted in designing the experiments, provided technical assistance and assisted in writing. SC and TV provided technical assistance with all experiments performed with *Physcomitrella patens*. RPK and PA provided technical assistance with confocal imaging and diverse phenotyping experiments, respectively. GG provided technical assistance on ultra-performance liquid chromatography-mass spectrometry (UPLC-MS) and performed data analysis. ON performed the auxin metabolite profiling. JJB performed the rootward auxin transport assays using radiolabelled [^{3}H]-IAA. KL, EZ and RN assisted in designing the experiments and complemented the writing. MKN complemented the writing. JF and JJB contributed to the experimental design and complemented the writing. BV and WB conceived the project, assisted in designing the experiments, supervised the experiments, and wrote the article.

FUNDING INFORMATION

This work has been supported by grants from the Hercules Foundation for the Synapt Q-Tof (grant no. AUGE/014), by the Multidisciplinary Research Partnership 'Biotechnology for a Sustainable Economy' (01MRB510W) of Ghent University and the Stanford University Global Climate and Energy Project ('Lignin management: optimizing yield and composition in lignin-modified plants'). SC is indebted to the Research Foundation Flanders for a predoctoral (3G032912) fellowship. WS is indebted to the Agency for Innovation by Science and Technology in Flanders (IWT) for a predoctoral fellowship. JF is supported by the European Research Council (project ERC-2011-StG-20101109-PSDP). RK acknowledges the OMICS@VIB post-doctoral program of the VIB. PK and EZ were supported by the Czech Science Foundation (project no. 16-10948S) and EU Operational Programme Prague - Competitiveness (project number CZ.2.16/3.1.00/21519), and ON acknowledges the Ministry of Education, Youth and Sport of the Czech Republic (the National Program for Sustainability I, grant no. LO1204). KL acknowledges the Swedish Governmental Agency for Innovation Systems (VINNOVA) and the Swedish Research Council (VR). RN acknowledges the support of BBSRC (BB/L009366), IC acknowledges the Foundation for Research of the State of São Paulo (FAPESP) for the Young Investigators Awards research fellowship (grant 2015/02527-1). PA acknowledges Conselho Nacional de Desenvolvimento Científico e Tecnológico (CNPq) fellowship (201998/2011-4).

CORRESPONDING AUTHOR EMAIL

bartel.vanholme@psb.vib-ugent.be
wout.boerjan@psb.vib-ugent.be

ABSTRACT

Auxin steers numerous physiological processes in plants making the tight control of its endogenous levels and spatiotemporal distribution a necessity. This regulation is achieved by different mechanisms including auxin biosynthesis, metabolic conversions, degradation and transport. Here we introduce *cis*-cinnamic acid (*c*-CA) as a novel and unique addition to a small group of endogenous molecules affecting *in planta* auxin concentrations. *c-CA* is the photo-isomerization product of the phenylpropanoid pathway intermediate *trans*-CA (*t*-CA). When grown on *c*-CA-containing medium, an evolutionary diverse set of plant species where shown to exhibit phenotypes characteristic for high auxin levels, including inhibition of primary root growth, induction of root hairs, and promotion of adventitious and lateral rooting. By molecular docking and receptor binding assays, we showed that *c*-CA itself is neither an auxin, nor an anti-auxin, and auxin profiling data revealed that *c*-CA does not significantly interfere with auxin biosynthesis. Single-cell-based auxin accumulation assays showed that *c*-CA, and not *t*-CA, is a potent inhibitor of auxin efflux. Auxin signaling reporters detected changes in spatiotemporal distribution of the auxin response along the root of *c*-CA-treated plants and long distance auxin transport assays showed no inhibition of rootward auxin transport. Overall, these results suggest that the phenotypes of *c*-CA-treated plants are the consequence of a local change in auxin accumulation, induced by the inhibition of auxin efflux. This work reveals a novel mechanism how plants may regulate auxin levels and adds a novel, naturally occurring molecule to the chemical toolbox for the studies of auxin homeostasis.

INTRODUCTION

Plant growth and development are tightly regulated by a plethora of signaling compounds, which are present within the plant at extremely low concentrations. Although the molecular working mechanism for several of these compounds has been described in detail (phytohormones, such as auxin and cytokinin, being among the best studied), for others the underlying mode of action is still unknown. Cinnamic acid (CA) is one of them and whereas the first report on its biological activity dates back to 1935 (Haagen-Smit and Went, 1935; Hitchcock, 1935), little additional research has been performed on this compound.

CA is found *in planta*, both as *trans (t)*- and *cis (c)*-isomers, though not in equal concentrations (Yang et al., 1999; Yin et al., 2003). *t*-CA is synthesized through the deamination of phenylalanine by PHENYLALANINE AMMONIA-LYASE (PAL) after which it is hydroxylated to *p*-coumaric acid by CINNAMIC ACID-4-HYDROXYLASE (C4H) (Boerjan et al., 2003). These are the first steps of the general phenylpropanoid pathway that lead towards a plethora of secondary metabolites such as flavonoids, stilbenes, tannins and monolignols (Vogt, 2010) (Fig. S1). Besides being a crucial intermediate of an important pathway, *t*-CA itself has also been described as a bioactive compound, though its exact activity has remained a matter of debate. Depending on the experiment, *t*-CA has been described as inactive, anta- or agonistic to auxin or an inhibitor of polar auxin transport (Van Overbeek et al., 1951; Åberg, 1961; Letham, 1978; Liu et al., 1993). *c*-CA is a photo-isomerization product of *t*-CA and, in contrast to the latter, is detected only in trace amounts in plants (Yin et al., 2003; Wong et al., 2005). However, it has been suggested to have higher biological activity compared to *t*-CA (Haagen-Smit, 1935). *c*-CA inhibits the gravitropic response of etiolated tomato seedlings and young tomato plants (Yang et al., 1999) and promotes cell-elongation in *Pisum sativum* (Haagen-Smit and Went, 1935; Koepfli et al., 1938; Went, 1939) and epinastic curvature of tomato plants (Yang et al., 1999). Although these effects resemble, to some extent, the physiological effects caused by perturbed auxin or ethylene homeostasis, further studies claimed that the mode of action of *c*-CA might be different from that of auxin and independent of ethylene-signaling (Yang et al., 1999; Wong et al., 2005).

In addition to this inconsistent view on the physiological role of CA in plants, an adequate explanation concerning the molecular mechanism by which both isomers independently affect plant growth and development is lacking. We evaluated the working mechanism of CA and demonstrate that *t*-CA is inactive as a molecular signal, consistent with its role as a primary intermediate in the general phenylpropanoid pathway. In contrast,

its *c*-isomer is biologically active and acts as a natural inhibitor of cellular auxin efflux, promoting lateral root formation.

176

RESULTS

1) CA affects plant development

An evolutionary diverse set of plant species was grown on tissue culture medium supplemented with commercially available CA and analyzed for aberrant growth phenotypes. In the higher land plants tested, CA inhibited primary root growth and induced the proliferation of adventitious and lateral roots in a dose-dependent manner (Fig. 1A and Supplemental Fig. S2A-D). In the Pteridophyte *Selaginella helvetica*, CA affected root apical meristem bifurcation, thickening of the root and root hair proliferation, resulting in a more dense root architecture (Supplemental Fig. S2E). In *Physcomitrella patens,* representing the Bryophytes, no clear effect on rhizoid growth was observed, but CA did stimulate cell and leaf elongation in the gametophores (Supplemental Fig. S2F-G). These results indicate that the addition of CA to the growth medium affects plant growth and development throughout the plant lineage.

To study the underlying molecular working mechanism of this compound we focused on *Arabidopsis thaliana.* In this model plant, the $IC_{50\text{-root}}$ value (i.e. the CA concentration needed to reduce the primary root length by 50%) was determined to be 9.2 µM under the conditions tested (Fig. 1B). Lateral root formation and adventitious rooting were stimulated, and the overall increase in number of emerged lateral roots combined with the reduction in primary root length resulted in a considerable increase in lateral root density (LRD). A 1.4 and 2.5 fold increase in LRD was obtained at applied CA concentrations of 2.5 and 5 µM, respectively (Fig. 1C). Concentrations above 10 µM resulted in the outgrowth of fasciated lateral roots along the primary root, and a significant increase in the number of adventitious roots (Fig. 1D-E). Besides, an increase in root hair number and length was observed not only on the primary root (Fig. 1F), but also on the lateral roots (Fig. 1G). Finally, a root waving phenotype was observed in CA-treated plants (Fig. 1A), indicating gravitropism defect. This was confirmed in a bending assay, revealing a dose-dependent perturbation of the gravitropic response by CA (Fig. 1H).

All experiments were performed with pure *t*-CA; however, photo-isomerization towards its *c*-isomer could not be excluded during these experiments. The light-mediated isomerization of CA is well described and is induced by UV-B (Hocking et al., 1969). Although UV-B radiation (280-315 nm) was detected in the growth chamber, the intensity was low (~0.02 W/m^2) and may not have been sufficient to increase the concentration of *c*-CA in the tissue culture medium during the growth period. To determine the isomerization efficiency under the applied plant growth conditions, 2.5 mg commercially available *t*- or *c*-CA was dissolved in 50 mL Milli-Q-H_2O/DMSO (80/20). Both solutions were subsequently placed in the growth chamber and the isomerization of both isomers was followed over time by ultra-high-pressure liquid chromatography (UHPLC)-mass spectrometry (MS). The chemical

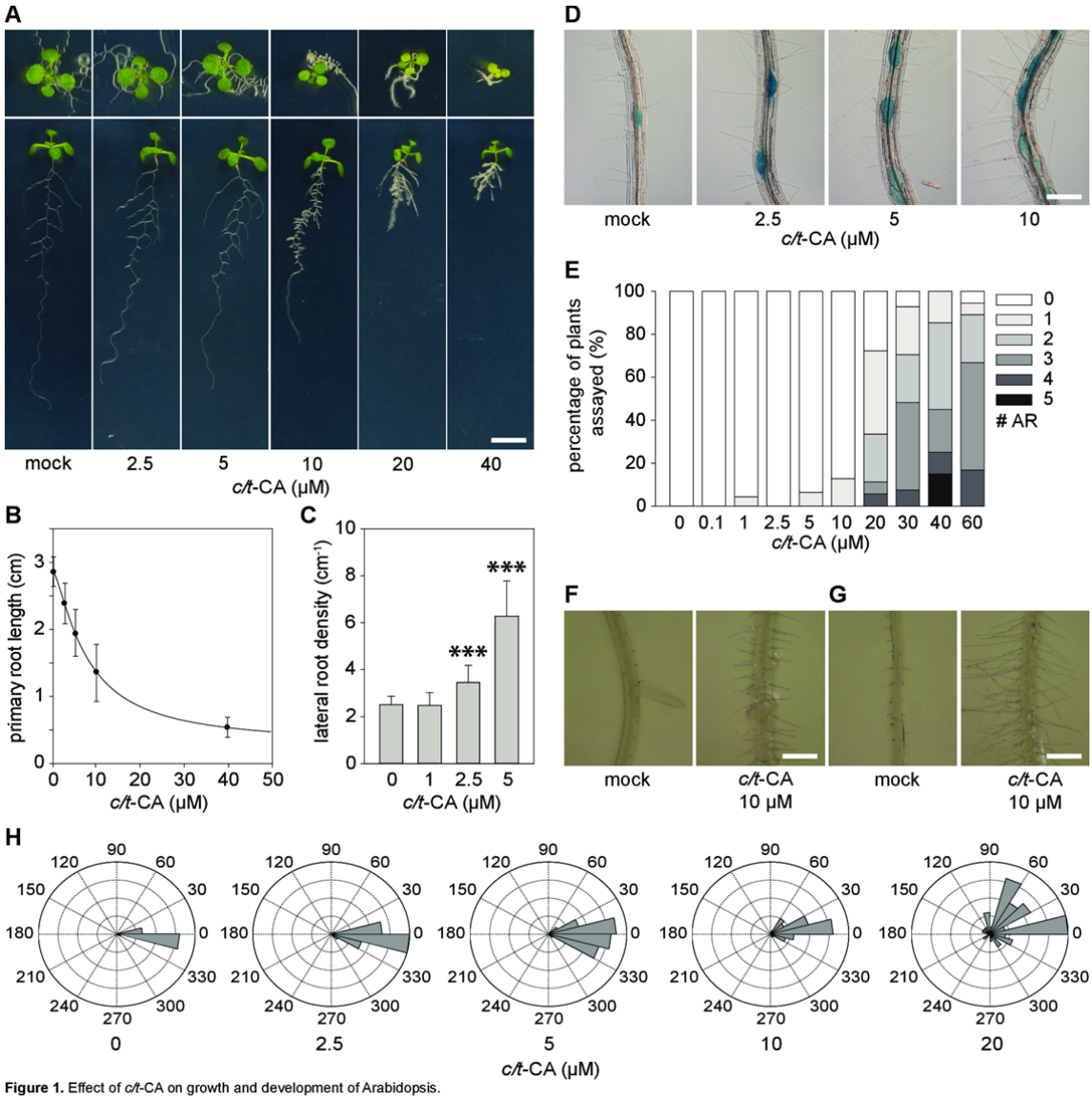

Figure 1. Effect of *c/t*-CA on growth and development of Arabidopsis.

(A) Root/rosette phenotype of representative seedlings 12 DAG, grown on 0.5xMS-medium supplemented with *c/t*-CA (n>20 for each concentration) (scale bar: 1 cm). (B) *c/t*-CA dose response curve for primary root growth (Sigmoidal-logistic, 4 parameters) (n>20). Error bars represent standard deviations. (C) Lateral root density of seedlings 12 DAG, grown on 0.5xMS-medium supplemented with *c/t*-CA (n>15). Error bars represent standard deviations and asterisks were used to indicate statistically significant differences compared to the corresponding mock-treated control sample as determined by Dunnett's test P-values: *P < 0.05, **P < 0.001, *** P <0.0001. (D) Representative light microscopic images of a root segment with lateral root primordia visualized by *CYCB1:GUS* expression in Arabidopsis 12 DAG of seedlings grown on 0.5xMS-medium supplemented with different concentrations of *c/t*-CA (n>10) (scale bar: 0.5 cm). (E) Number of adventitious roots of seedlings 12 DAG grown on 0.5xMS-medium supplemented with *c/t*-CA. Plants were grown for 7 days in darkness (after a short light-pulse of 4h with red-light to induce germination) and subsequently transferred to light to stimulate adventitious rooting. Adventitious root numbers are represented in grey-scale (n>20). (F-G) Binocular microscopic images of a root segment of the (F) primary root and (G) lateral root of seedlings 12 DAG, grown on 0.5xMS-medium whether or not supplemented with 10 µM *c/t*-CA (n=10). (H) Histogram showing the *c/t*-CA-induced disruption of the gravitropic response in the main root. Seeds were germinated on 0.5xMS-medium and 4 DAG seedlings were transferred to 0.5xMS-medium supplemented with *c/t*-CA. Subsequently, seedlings growing on vertical plates were rotated 90 degrees and each root was assigned to one of 12 30° sectors after 48h incubation (n>25).

equilibrium was in favor of the *c*-isomer (57%) and was reached after 8 or 15 days, depending on the use of *c*-CA or *t*-CA as the initial compound (Supplemental Fig. S3). This indicates that despite the application of *t*-CA to the growth medium, a substantial amount of the *c*-isomer could be expected during the period of plant growth. Consequently, the observed growth defects could not be linked unambiguously to the presence of *t*-CA in the medium.

No spontaneous isomerization was detected in the dark, under deep-red (650-670nm), or far-red illumination (725-750nm). Therefore, experiments to reveal the effect of

the pure isomers could be performed under these conditions. To distinguish the experiments performed with *t*-CA in the dark from experiments performed in the light, the latter will be indicated as *t/c*-CA here onwards, although *t*-CA was added to the tissue culture medium for both experiments.

Knowing the photo-isomerization conditions, we questioned if both isomers had similar biochemical properties. Arabidopsis seeds were placed on 0.5×MS-medium supplemented with either pure *c*-CA or *t*-CA and incubated in darkness to avoid photo-isomerization. Twelve days after germination (DAG) seedlings were screened for phenotypes as before. Whereas no effect on the elongation of the hypocotyl was observed (Fig. 2A), an inhibitory effect on primary root growth was evident (Fig. 2B). Here *c*-CA was much more effective than *t*-CA ($IC_{50\text{-root}}$ of 3.2 µM and 82.4 µM for *c*- and *t*-CA, respectively). To test the metabolism of *t*- versus *c*-CA, a yeast heterologous expression system was used to express Arabidopsis C4H. In contrast to *t*-CA, *c*-CA was not converted to *p*-coumaric acid by Arabidopsis C4H (Supplemental Fig. S4).

Therefore, only *t*-CA is an intermediate in the general phenylpropanoid pathway. The *c*-isomer is the biologically active isomer affecting a number of developmental processes *in planta* and it is likely that most if not all physiological effects that have been previously attributed to the *t*-CA isomer or CA in general, are caused by *c*-CA.

2) *c*-CA affects root architecture

In Arabidopsis, lateral roots arise from asymmetric anticlinal divisions of founder cells in the pericycle layer basal to the main root meristem (De Rybel et al., 2010). As *c*-CA causes lateral root proliferation (Fig. 1D), the effect of *c*-CA on cell division in this cell layer was studied in more detail using the cell plate marker KNOLLE. An increase in the expression of *KNOLLE*-driven *GFP* was observed along the pericycle of 7 day old dark-grown seedlings treated for 3 days with 10 µM *c*-CA, confirming strong induction of mitotic activity in this cell layer upon addition of *c*-CA (Fig. 2C). Notably, prolonged treatment for 3 days with 10 µM *c*-CA resulted in epidermal and cortical cell peeling (Fig. 2C) suggesting active degradation of the pectin-rich middle lamella between adjacent cells. POLYGALACTURONASE ABSCISSION ZONE ARABIDOPSIS THALIANA (PGAZAT) mediated pectin degradation is known to be important for lateral root outgrowth (Gonzalez-Carranza et al., 2007; Kumpf et al., 2013) and the *PGAZAT* promoter turned out to be strongly activated by 10 µM *c*-CA in cortical and epidermal cell layers surrounding developing lateral roots, but not in the lateral roots themselves (Fig. 2D). The active cell wall remodeling in the epidermis and cortex will facilitate the outgrowth of the *c*-CA induced lateral roots.

Both the *KNOLLE* and *CYCB1* reporter lines highlighted the effect of *c*-CA on the left-right alternation and spatial organization characteristic for Arabidopsis lateral roots (Fig. 1D

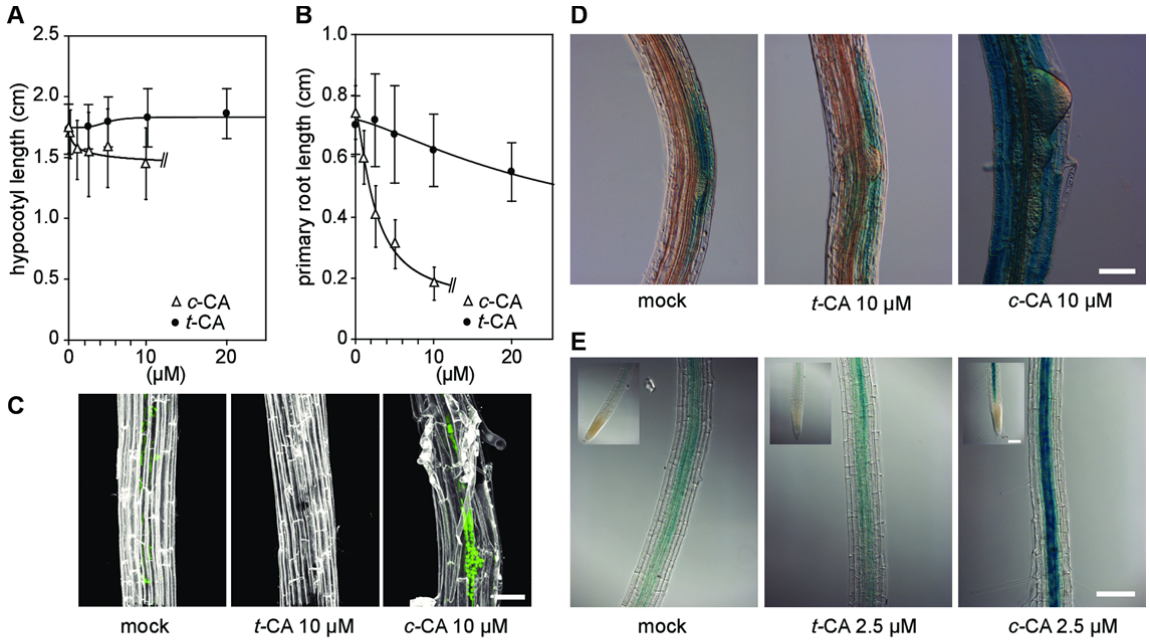

Figure 2. Effect of *c*-CA on root architecture.

Dose response curves (Sigmoidal-logistic, 4 parameters) showing the effect of *c*-CA (triangles) or *t*-CA (dots) on (A) hypocotyl and (B) root length of seedlings 12 DAG, grown in darkness on 0.5xMS-medium supplemented with either *c*- or *t*-CA (n>20). Seed germination was induced by a 4h red light-pulse. (C) Confocal images showing *KNOLLE* promoter activity (green) of 10 DAG *pKNOLLE:KNOLLE-GFP* seedlings. (D-E) Light microscopic images of *c*-CA induced GUS activity in 10 DAG *pPGAZAT:GUS* and *pGATA23:GUS* seedlings. GUS activity was monitored at the lateral roots (PGAZAT) or the zone basal to the main root tip (GATA23). For the *GATA23* driven GUS expression the main root tip is shown as inset. For (C) and (D), seeds were germinated on 0.5xMS-medium and 7 DAG seedlings were transferred to 0.5xMS-medium supplemented with 10 µM *c*-CA or *t*-CA (n=5) (scale bar: 15 µm).Growth conditions for (E) were as for (C) with the only exception that *c*-CA and *t*-CA were used at 2.5 µM (n=5).

and Fig. 2C). The altered root pattern could originate at the level of lateral root founder cell specification, which occurs in the basal meristem before the initial anticlinal division of the founder cells (De Rybel et al., 2010). To visualize the effect of *c*-CA on lateral root priming we used a reporter line harboring the promoter of the GATA23 transcription factor fused to a *GUS* reporter. *GATA23* expression is considered as hallmark of the earliest steps in lateral root formation (De Rybel et al., 2010). In mock-treated plants, *GUS* expression was observed in pericycle cells starting close to the root tip and continued along the root in a zone lacking emerged lateral root primordia. Treating the marker line 5 days after germination (DAG) with 2.5 µM *c*-CA for 21 hours resulted in ectopic and enhanced GUS activity stretching continuously from the main root tip onwards till the maturation zone. In addition, local patches of strong GUS activity were observed, most likely corresponding to founder cell formation in pericycle cells adjacent to xylem pools (Fig. 2E and Supplemental Fig. S5).

These results reveal that *c*-CA triggers cell priming, which initiates lateral root proliferation. *t*-CA included in each set of experiments for comparison, never induced an effect different from the mock-treatment, supporting our previous finding that the biological activity of CA is restricted to its *c*-isomer.

3) *c*-CA triggers an auxin response

Lateral root proliferation is a classical auxin-mediated process. To disclose putative crosstalk between *c*-CA and auxin, we monitored whether *c*-CA could affect the local auxin

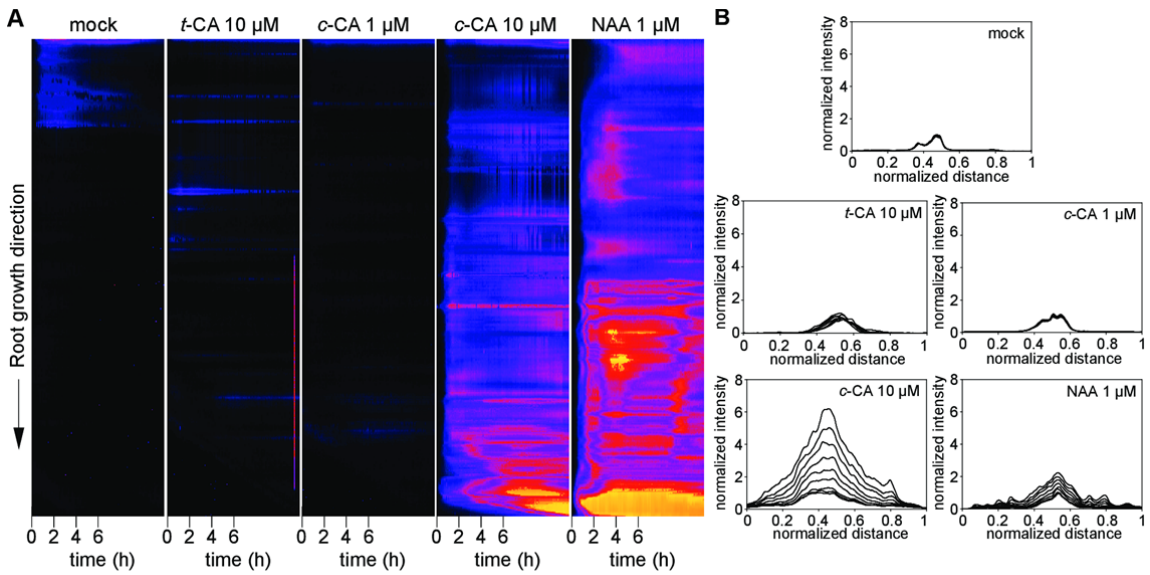

Figure 3. *c*-CA induces an auxin response in Arabidopsis.

(A) Kymograph of *pDR5:LUC* intensity along the primary root of Arabidopsis seedlings during a 12h period. The kymograph represents on the vertical axis the primary root, with the root tip present in the orignin of the coordinate system, and the shoot/root junction at the end of the vertical axis. The horizontal axis represents time. Seeds were germinated on 0.5xMS-medium and 5 DAG seedlings were transferred to 0.5xMS-medium supplemented with 1-10 µM *c*-CA, 10 µM *t*-CA or 1 µM NAA. Imaging was started at the moment of transfer and data was recorded every 10 minutes. Each kymograph represents one experiment. The kymograph is representative for 8 biological repeats (seedlings). B) Confocal time-lapse imaging of *pDR5rev:GFP* intensity in the primary root between two young emerged lateral roots. At the start of the time-lapse, seedlings were placed in glass-bottomed dishes and covered with 0.5xMS-medium containing 1 µM NAA, 1-10 µM *c*-CA or 10 µM *t*-CA. The time-lapse was started 5 minutes after the seedlings had been placed in contact with the media and captured every 60 minutes over a 16h period. Cumulative spectra were obtained by projecting the GFP intensity on a virtual line crossing the middle of the primary root. Normalization was performed against the maximal intensity of the signal at the earliest time point (n=1). Each spectrum is representative for 3 biological repeats (positions along the primary root).

response along the primary root using the auxin response reporter *DR5:LUC* (Moreno-Risueno et al., 2010). Arabidopsis seedlings were transferred 5 DAG to 0.5xMS-medium supplemented with the compound of interest and luciferase activity was monitored every 10 minutes over a 12h time interval. In mock-treated plants, luciferase activity was seen in the shoot/root apical meristems, and lateral root initiation sites. This spatial pattern is in line with the described distribution of auxin maxima along the primary root of Arabidopsis seedlings (Benkova et al., 2003). Supplying the medium with 10 µM *t*-CA did not affect this pattern, whereas the addition of 1 µM naphthalene-1-acetic acid (NAA) resulted in a strong increase in luciferase activity along the primary root from the first time point onwards, and the signal intensity increased over time (Fig. 3A and Supplemental Fig. S6). Similar to NAA, *c*-CA caused an increase in the luciferase signal in a dose-dependent manner. When supplied at 10 µM, the signal accumulated along the primary root. However, after 6 hours the luciferase activity dropped in the root maturation zone, but remained in the lateral root primordia and the primary root tip, where the signal accumulated to saturation levels. This spatial distribution was highly similar to that obtained with a lower *c*-CA dose (5 µM), although the whole process was slower and never reached saturation during the timespan of the experiment. (Fig. 3A and Supplemental Fig. S6).

Besides the spatial shift of the *c*-CA-induced *DR5*-driven signal along the longitudinal axis of the root, an axial redistribution of the signal was observed as well. To follow and quantify this lateral distribution over time we shifted to 4D microscopy using *DR5rev:GFP*

seedlings (Friml et al., 2003), grown and treated as for the *DR5:LUC* experiment. After transferring seedlings 5 DAG to the *c*-CA-containing medium (10 µM), the region between two young emerged lateral roots was scanned every hour over a 16h period. At the second time point (2h) a significant increase in fluorescence was observed in the stele, increasing with time, and expanding across the pericycle into neighboring cell layers (Fig. 3B and Supplemental Fig. S7). A comparable pattern was obtained with 1 µM NAA (included as positive control), although the fluorescence at the end of the observation period was lower as compared to that achieved with *c*-CA-treated roots (Fig. 3B and Supplemental Fig. S7).

These observations show that *c*-CA has auxin-like effects on plant development and affects the spatial distribution of the auxin response at low micro molar concentrations.

4) *c*-CA does not act as a typical auxin

The overall similarity in *DR5*-driven fluorescence between *c*-CA- and NAA-treated plants suggests that *c*-CA functions via the TRANSPORT INHIBITOR RESPONSE1/AUXIN SIGNALING F-BOX (TIR1/AFB) auxin-signaling pathway (Peret et al., 2009). To investigate whether *c*-CA acts via this canonical auxin-signaling pathway, we grew the *solitary root-1 (slr)* gain-of-function Aux/IAA mutant and the *arf7 arf19* double mutant on *c/t*-CA-supplemented medium. Like auxin, *c/t*-CA failed to induce lateral root formation in these mutants, suggesting that *c*-CA functions upstream of these steps in the auxin signaling cascade toward lateral root formation (Fig. 4A). As SLR1/IAA14 is a direct target of the auxin receptor TIR1, we subsequently tested whether TIR1 was essential for *c*-CA activity by growing the *tir1 afb2 afb3* mutant on *c/t*-CA containing medium. As for the other mutants testedno lateral roots were induced in this mutant indicating that the TIR1 auxin receptor is crucial for this *c*-CA-mediated growth defect (Fig. 4A). Based on these observations we concluded that *c*-CA could be an auxin analogue that induces the auxin signaling cascade by interacting with the TIR1 auxin receptor in a similar way as the native auxin, indole-3-acetic acid (IAA). However, simulation of the molecular docking of *c*-CA in the auxin receptor pocket of TIR1 revealed a position different from the experimentally determined orientation of IAA (Supplemental Fig. S8). To validate the prediction, the interaction kinetics of TIR1 and the related AFB5 with immobilized peptides corresponding to the degron motif of Aux/IAA7 were followed using Surface Plasmon Resonance (SPR). Whereas strong signals were obtained with IAA and NAA used as a positive controls, no evidence for a specific binding of *c*-CA or *t*-CA to the auxin receptors was found (Fig. 4B). Both isomers were also tested for anti-auxin activity. Although such property was claimed for *t*-CA (Van Overbeek et al., 1951), no supporting evidence for such activity was found (Fig. 4B).

Together, these results indicate that neither CA-isomer acts as an auxin agonist, nor an antagonist at the level of the auxin perception and support the hypothesis that *c*-CA acts

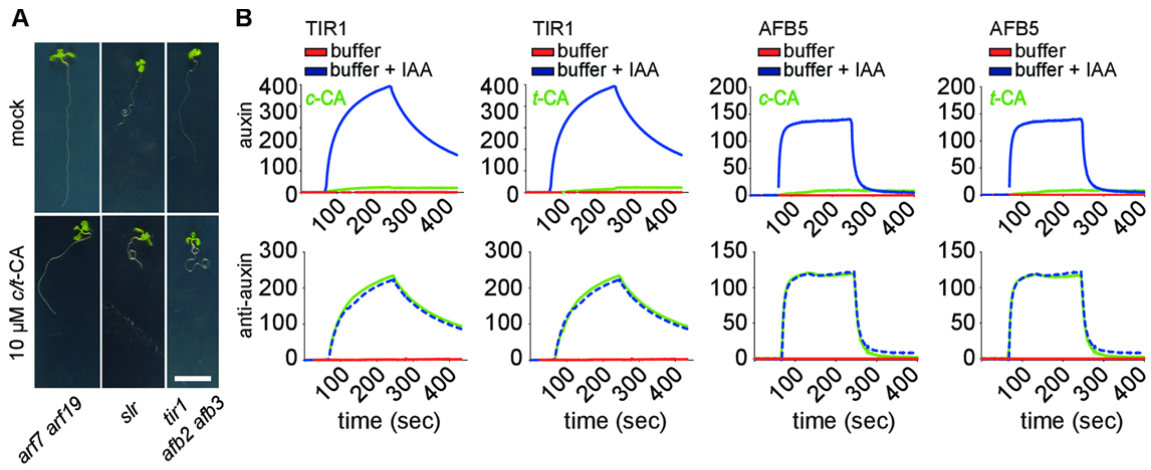

Figure 4. *c*-CA does not act as a typical auxin.

(A) Root phenotype of *arf7 arf19*, *slr* and *tir1 afb2 afb3* mutants 12 DAG, growing on 0.5xMS medium supplemented with 10 µM *c/t*-CA (n>25) (scale bar: 1 cm). (B) Surface Plasmon Resonance sensorgrams showing the auxin-depended interaction between TIR1 or AFB5 with IAA DII. Each sensorgram shows the binding with IAA (blue), an auxin-free injection (red) plus the data for each test compound (green). For auxin activity assays (top) compounds (50 µM) were mixed with TIR1 or AFB5 prior to injection over DII peptide. For anti-auxin assays (bottom), compounds (50 µM) were mixed with TIR1 or AFB5 plus 5 µM IAA prior to injection. The degron sequence that was used : biot-AKAQVVGWPPVRNYRKN.

via an auxin-dependent pathway for lateral root formation by modifying auxin homeostasis or the spatiotemporal distribution of auxin in roots.

5) *c*-CA triggers lateral root formation in an auxin-dependent manner

To assess whether activation of the *DR5* promoter is due to an overall shift in IAA concentrations, UHPLC-MS profiling was performed on Arabidopsis seedlings 12 DAG. Before the extraction plants were treated with 10 µM *c*-CA or *t*-CA for 1 and 6 hours (Supplemental Fig. S9 and S10). No major shifts in the IAA metabolome were observed between *t*-CA- and mock-treated plants again confirming the absence of bioactivity for this compound. For the *c*-CA-treatment an effect was observed 6 hours after the transfer of the seedlings to 10 µM *c*-CA (Supplemental Fig. S10). At this point a small, but significant increase in indole-3-acetamide, indole-3-acetonitrile, and indole-3-acetaldoxime was observed. In addition, intermediates of the indole-3-pyruvic acid (IPyA)-pathway for IAA biosynthesis accumulated in seedlings treated with *c*-CA for 6 hours. This pattern could be transient as no significant increase in free IAA levels or in any of its conjugates was detected after 6 hours. The absence of a clear shift in free IAA levels in combination with the observed rapid and strong activation of the *DR5* promoter questions the importance of auxin biosynthesis for *c*-CA-induced lateral root formation. The role of IAA itself was reconsidered by testing lateral root induction in plants with artificially reduced IAA levels using the IAA lysine synthase (iaaL) overexpressing line. The bacterial *IAAL* gene encodes an enzyme which inactivates IAA by conjugating it to the amino-acid lysine. Seeds from the *p*35S:*iaaL*-line were germinated as above and LRD was quantified 12 DAG. When treated with *t/c*-CA, *p*35S:*iaaL* plants showed fewer lateral roots than WT plants, indicating that *c*-CA-induced lateral root induction is indeed mediated by free IAA (Supplemental Fig. S11).

In summary, the bioactivity of *c*-CA is clearly dependent on auxin. The fact that free IAA is not increased in *c*-CA-treated plants suggests that auxin is redistributed within the plant, resulting in novel auxin maxima that inhibit primary root growth and promote lateral root development.

6) *c*-CA inhibits cellular auxin efflux

The ability of *c*-CA to induce an auxin response via the canonical auxin-signaling pathway without being a receptor agonist suggests that *c*-CA interferes with tightly controlled auxin concentrations in the plant. To obtain insight into possible *c*-CA-mediated dynamic changes of auxin responses at high spatial resolution in a short time-interval the visual marker DII-VENUS was used (Brunoud et al., 2012). A time-course was recorded of DII-VENUS fluorescence in the primary root tip of Arabidopsis seedlings 7 DAG. Forty-five minutes after the addition of 1 μM NAA DII-VENUS fluorescence dropped to 25% of its initial intensity (Fig. 5A and Supplemental Fig. S12), which is in line with previously published data (Brunoud et al., 2012). The DII-VENUS sensor reacted in a similar way following treatment with *c*-CA, although compared to NAA a 10-fold higher concentration of *c*-CA was required to reduce the fluorescence to a comparable level (i.e. 29% of the initial fluorescence after 42 minutes with 10 μM *c*-CA; Fig. 5A and Supplemental Fig. S12). Remarkably, also *t*-CA turned out to be active in this assay, which contradicts previous findings claiming activity restricted to the *cis*-isoform. However, the *t*-CA mediated reduction of DII-VENUS signal is most likely a direct consequence of laser mediated isomerization of *t*-CA towards *c*-CA during imaging (so called photo-activation). Lowering the concentration of *c*-CA to 1 μM resulted in a pattern indistinguishable from that of mock-treated samples during the initial time points. Intriguingly, after 10 minutes the pattern started to deviate from the negative control and a slight increase in DII-VENUS degradation could be observed. This trend was sustained and resulted in a significant drop in fluorescence by the end of the experiment. Interestingly, DII-VENUS degraded at a similar speed as in the samples treated with the higher concentration of *c*-CA (Fig. 5A). This peculiar profile could indicate that *c*-CA interferes with auxin transport. This would lead to increasing intracellular auxin concentrations and consequent DII-VENUS degradation once a critical auxin concentration threshold is passed. To find supporting evidence for this hypothesis the experiment was repeated with 1-naphthylphthalamic acid (NPA), a well-established inhibitor of auxin efflux. As for *c*-CA, NPA caused a dose-dependent reduction in DII-VENUS fluorescence with similar dynamics as after treatment with *c*-CA, indicating that both these compounds similarly increase auxin accumulation in the primary root tip (Supplemental Fig. S13). In line with the proposed model, at the lower concentrations tested (0.1 and 1.0 μM NPA), a pattern was obtained which only deviated

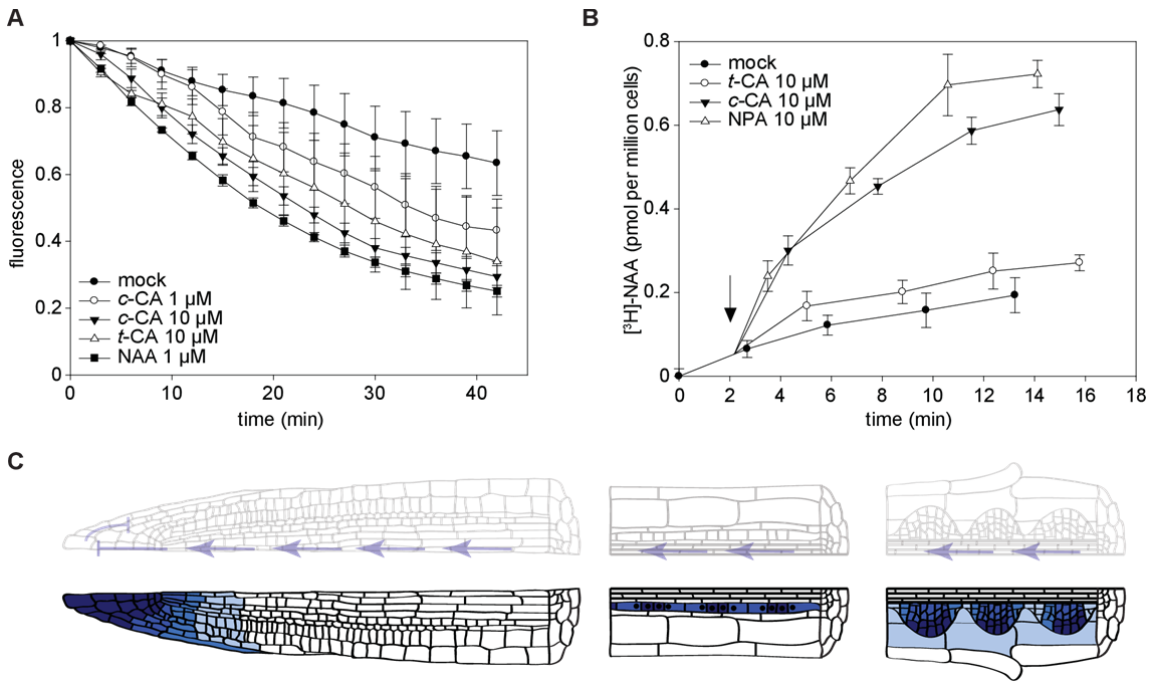

Figure 5. Effect of *c*-CA on polar auxin transport.

(A) Time-course of DII-VENUS fluorescence in the main root tip of *DII-VENUS-YFP* seedlings. Plants were germinated on 0.5xMS-medium and subsequently transferred 5 DAG to 0.5xMS-medium supplemented with 1 or 10 µM *c*-CA, 10 µM *t*-CA or 1 µM 1-NAA (n=3). (scale bar: 50 µm). Fluorescence was quantified every 3 minutes over a 42 minute period. During each experiment 3 root tips (representing one treatment) were simultaneously imaged. Error bars represent standard deviations. (B) Effect of 10 µM *c*-CA, *t*-CA or NPA on the net accumulation of [^{3}H]-NAA in 2-day old suspension-cultured tobacco BY-2 cells (20 minute uptake period). The arrows points to the time of application of the compound. Error bars represent standard deviations (n=4). (C) Model explaining the *c*-CA mediated lateral root proliferation. *c*-CA inhibits shootward auxin transport by inhibiting the redistribution of auxin in the meristem. This is considered a direct consequence of the *c*-CA mediated inhibition of auxin efflux. The phloem-mediated rootward auxin transport in the primary root is not disturbed by *c*-CA, allowing a continuos supply of auxin from the shoot towards the root tip. The block of a proper auxin redistribution in the meristem results in the accumulation of auxin in the primary root, where it triggers lateral root proliferation. Top: auxin flow (blue arrows) and its perturbation within the primary root of *c*-CA treated plants. Bottom: schematic represenatiation of auxin accumulation in the primary root of *c*-CA treated plants and the consequent induction of lateral roots.

from the mock-treated control after a temporal delay, of which the length was dependent on the NPA concentration (Supplemental Fig. S13).

The putative link between *c*-CA and polar auxin transport machinery was further explored by auxin accumulation assays on the cellular level. Polar auxin transport depends on the localization and activity of auxin influx and efflux carriers (Adamowski and Friml, 2015). In tobacco cells, NAA enters the cells mainly by diffusion (Delbarre et al., 1996; Hoyerova et al., 2011), whereas it is an excellent substrate for active efflux. Therefore, a change in intracellular accumulation of radioactively-labeled NAA in BY-2 tobacco cell-suspension culture over time provides a measure of the activity of auxin efflux from cells (Fig. 5B). Control cells displayed [^{3}H]-NAA accumulation kinetics indicative of active and saturable auxin-efflux (Petrasek et al., 2006). After treatment with NPA [^{3}H]-NAA accumulated strongly inside the cells, and a similar although slightly reduced response was obtained when NPA was replaced with *c*-CA, indicating that *c*-CA acts as a potent inhibitor of auxin efflux. This increase in accumulation was not observed upon treatment with *t*-CA (Fig. 5B). When a similar experiment was performed with a combination of NPA and *c*-CA, [^{3}H]-NAA accumulated to a similar level as in NPA-treated cells, indicating *c*-CA targets a subset of NPA-sensitive auxin transporters (Supplemental Fig. S14), which could be either PIN-FORMED (PIN) or ATP-binding cassette-B (ABCB) transporters (Petrasek et al., 2009). To

distinguish between both, NPA was substituted for the ABCB-specific inhibitor 2-[4-(diethylamino)-2-hydroxybenzoyl] benzoic acid (BUM) (Kim et al., 2010). In contrast to NPA, BUM inhibited auxin efflux to the same extend as *c*-CA in the auxin transport assay, and no additive effect was observed when BUM and *c*-CA were used simultaneously (Supplemental Fig. S15). This strongly suggests *c*-CA targets predominantly the ABCB-auxin transport machinery. To test whether *c*-CA might also affect auxin influx, [^{3}H]-NAA was replaced for [^{3}H]-2,4-D, which is a preferred substrate for influx activity. When added to the BY-2 cell suspension, [^{3}H]-2,4-D accumulated in the cells until a plateau was reached, representing equilibrium between cellular influx and efflux of the labeled compound (Supplemental Fig. S16). Using this experimental setup we found no indication that either *c*-CA or *t*-CA affects cellular auxin influx.

Based on these experiments, we concluded that *c*-CA, but not *t*-CA, inhibits auxin efflux from cells, more specifically the ABCB-mediated part of auxin efflux. The consequent accumulation of intracellular auxin could be at the basis of the physiological and developmental defects observed in *c*-CA-treated Arabidopsis seedlings.

7) *c*-CA does not inhibit long-distance rootward auxin transport

Although both NPA and *c*-CA block cellular auxin efflux, their effects on Arabidopsis roots are entirely different. NPA arrests (Casimero et al., 2001; Benkova et al., 2003) and *c*-CA induces lateral root formation. Supported by the spatiotemperal distribution of *DR5* driven luciferase activity we hypothesized that a difference in long-distance auxin transport could be the origin of the phenotypic difference between these two auxin efflux inhibitors. Whereas NPA affects both rootward and shootward auxin transport in the primary root (Casimero et al., 2001), the strong increase in luciferase activity in the tip of *c*-CA-treated roots suggested that rootward auxin transport is not disturbed by *c*-CA. To verify this hypothesis, we monitored whether local *c*-CA application could affect distant auxin-inducible luciferase activity using a split medium approach as described by Lewis and Muday (2009). To this end, seedlings were positioned on the medium in a way that either the upper or the lower half of the root was in contact with *c*-CA. Dynamics of luciferase activity along the root were followed over time as described above. When the lower half of the root was in contact with *c*-CA, luciferase activity accumulated in the root tip in line with earlier data (Supplemental Fig. S17). When only the upper part of the root was in contact with *c*-CA, the luciferase signal quickly extended towards the non-treated zone (Supplemental Fig. S17). This illustrates that auxin appears to be able to pass through the *c*-CA-treated zone in a rootward direction.

Although the data support the hypothesis that *c*-CA allows long-distance rootward auxin transport, we could not exclude an alternative explanation, namely that *c*-CA itself is transported and triggers auxin signaling locally. To provide undisputed evidence for rootward

transport of auxin in *c*-CA treated roots, long-distance rootward auxin transport was assayed in primary roots of Arabidopsis seedlings in which the roots were exposed to either mock or *c*-CA-treated 0.5xMS-medium. In these assays, microdroplets of radiolabelled [^{3}H]-IAA were placed precisely on the shoot apical meristems of Arabidopsis seedlings and rootward auxin transport was measured by harvesting a 4 mm segment centered on the root/shoot transition zone, as well as the entire root, in 2 mm segments. Consistent with previous results, treatment with *c*-CA did not inhibit rootward auxin movement (Fig. 5C and Supplemental Fig. S18). The strong accumulation of the auxin-inducible luciferase in the root tip is characteristic of the inhibition of shootward auxin transport (Fig. 3A and Supplemental Fig. S6 and S17). Unfortunately, reliable data were not obtained for shootward auxin transport to support this hypothesis.

Taken together, our data supports a model (Fig. 5C) in which *c*-CA inhibits auxin efflux at the cellular level in specific cells at or near the root apical meristem, while allowing long-distance rootward auxin transport at the organ level. The resultant accumulation of auxin in the root apical meristem might cause, at least in part, the observed growth defects induced by *c*-CA.

DISCUSSION

Being sessile organisms, plants cannot escape unfavorable growth conditions. This shortcoming is compensated by an extreme plasticity allowing them to react on changing environmental cues. Here, the phytohormone auxin has an important function as it is key in the regulation of many processes involved in growth and development (Vanneste and Friml, 2009). As for all bioactive compounds, tight regulation of its homeostasis and spatiotemporal distribution inside the plant is crucial, as suboptimal auxin concentrations will not trigger the desired response, while high concentrations will be harmful. The ability to control auxin levels is a necessity for plant survival and occurs at the cellular level by regulating biosynthesis, metabolic conversions as well as degradation, whereas transport is essential to translocate auxin between different cells and tissues. Synthetic inhibitors of auxin transport such as NPA and BUM have proven the importance of this process in diverse physiological actions, including embryogenesis, tropisms, vascular patterning and lateral root initiation (Kim et al., 2010). Intriguingly, endogenous auxin transport inhibitors are scarce. Flavonols and flavonoids such as quercetin were considered to inhibit auxin transporters (Brown et al., 2001) although later work suggested that flavonoids also act by redirecting PIN efflux protein localization (Santelia et al., 2008). Certain flavonoid mutants display auxin-related defects (Buer et al., 2013) and an auxin-transport inhibiting activity was recently assigned to the flavonol glycoside kaempferol 3-*O*-rhamnoside-7-*O*-rhamnoside (Yin et al., 2014).

Here we introduce *c*-CA as a novel endogenous inhibitor of auxin transport. Intriguingly, the activity of *c*-CA resembles that of NPA but only at the cellular level. Although both NPA and *c*-CA block cellular auxin efflux, the effects of the two compounds on Arabidopsis root architecture are entirely different, with *c*-CA inducing lateral root formation and NPA impacting several auxin-dependent phenotypes, including lateral root initiation. The exact mechanism of NPA action is still unknown, but according to one hypothesis the *solitary root* phenotype of NPA-treated plants is a consequence of auxin depletion in the root due to the perturbation of basipetal and acropetal auxin transport (i.e. shootward and rootward, respectively) (Casimiro et al., 2001). While, explaining the observed phenotype, the molecular mechanism underlying the inhibition of phloem-based (and hence no-transporter mediated) rootward auxin transport by an auxin efflux inhibitor remains unknown. Proceeding from this model we hypothesized that a difference at the level of rootward transport (blocked by NPA but not by *c*-CA) underlies the phenotypic differences caused by the two compounds. Under mock conditions, auxin is redistributed in the root tip according to the "reverse-fountain" model, in which specific auxin transport proteins (PINs and ABCB proteins) play distinct roles in establishing directional movement of auxin (Benkova et al., 2003; Blilou et al., 2005; Lewis and Muday, 2009). By inhibiting cellular auxin efflux, we hypothesize *c*-CA will affect the auxin reflux in the meristem resulting in the inhibition of

shootward auxin transport. Consequently, auxin either transported from the shoot or synthesized in the primary root tip will accumulate behind the root tip where it will trigger GATA23-expression and affect lateral root founder cell specification. Over time, the accumulating auxin will enter pericycle cells, either by diffusion or active influx where it will be trapped due to the *c*-CA mediated inhibition of auxin efflux, similar to the situation in the primary root. Once the auxin concentration passes a critical threshold, primed cells will be triggered to develop into lateral root founder cells, which eventually will develop into new lateral roots, shaping the altered root architecture (Fig. 5C).

Compared to NPA, *c*-CA was found slightly less efficient in the auxin accumulation assay. This difference may result from the broader specificty of NPA, known to affect different types of auxin efflux carriers. Based on the absence of an additive effect of *c*-CA and BUM in this assay we concluded that *c*-CA targets the ABCB subfamily of the multi-drug resistent/P-glycoprotein (MDR/PGP) integral membrane proteins. These transporters are well known for their capacity to pump drugs out of the cell (Kang et al., 2011), increasing the resistance of the cell and hence the organism towards compounds that are considered toxic under normal conditions. Interestingly, and in line with our observation, the *cis*-form of CA and not its *trans*-form raises a notable synergistic bactericidal activity against multiple-drug resistant *Mycobacterium tuberculosis*. It is tempting to speculate that also in this case *c*-CA blocks the MDR-transporters, resulting in the intracellular accumulation of the supplied antibiotics to levels required to kill the bacteria (Chen et al., 2011).

Although the physiological role of endogneous *c*-CA is still unclear, the beauty of this bioactive molecule lies in the fact that it can be produced from a readily available inactive compound (*t*-CA) by sunlight (Ding et al., 2011). This gives a tremendous opportunity to link environmental conditions directly to developmental regulation without the need to activate gene expression to alter the auxin pool. In addition, we cannot exclude that a similar conversion can be obtained by a yet-to-be-discovered enzyme, further extending the possibilities to exploit this mechanism to steer plant development independently of light. The question of whether or not *c*-CA has an active role in the regulation of plant development remains an open and intriguing question; however, the fact that it was previously found in small but physiologically relevant quantities in plants and that the effects on roots are evolutionary conserved, only feeds the speculation on its importance as an endogenous plant growth regulator (Yin et al., 2003; Wong et al., 2005). This function could be different from lateral root development, a system that we only used to elucidate the molecular mechanism of *c*-CA action.

MATERIAL AND METHODS

Plant material, transgenic lines, chemicals and growth conditions

The effect of *c/t*-CA on plant growth and development was studied in a diverse set of plant species, comprising *Physcomitrella patens*, *Selaginella helvetica*, *Oryza sativa, Nicotiana benthamiana*, *Brachypodium distachyon*, and *Arabidopsis thaliana*. *Arabidopsis thaliana* ecotype Columbia (Col-0) was used, unless stated elsewhere. The used transgenic lines were in the same ecotype: DII-VENUS, *DR5rev:GFP*, *DR5:LUC*, *pGATA23:GUS*, *pGAZAT:GUS*, *pKNOLLE:KNOLLE-GFP*, *p35S:iaaL*, *slr*, *arf7 arf19* and *tir1 afb2 afb3* (Romano et al., 1991; Lukowitz et al., 1996; Fukaki et al., 2002; Friml et al., 2003; Dharmasiri et al., 2005; Gonzalez-Carranza et al., 2007; Okushima et al., 2007; De Rybel et al., 2010; Moreno-Risueno et al., 2010; Brunoud et al., 2012*)*. The transgenic line pCYCB1:GUS was in the ecotype Landsberg Erecta (Ler) (Colon-Carmona et al., 1999). Seeds were vapor-phase sterilized and grown on 0.5xMS-Medium. 0.5xMS medium (pH 5.7) contains per liter 1.5 g Murashige and Skoog basal salt mixture powder (Duchefa), 7.14 g sucrose, 0.36 g MES monohydrate, 8 g plant tissue culture agar. The medium was supplemented with one of the following compounds: naphthalene-1-acetic acid (NAA; Sigma Aldrich), 1-naphthylphthalamic acid (NPA; Sigma Aldrich), *c*-CA (Shanghai Specbiochem CO., LTD) and *t*-CA (Sigma Aldrich) from stock solutions in dimethyl sulfoxide (DMSO) (final 0.1% DMSO) to the autoclaved medium prior to pouring the plates. After sowing, seeds were incubated at 4°C for at least 2 days whereupon plates were placed in a vertical orientation in the tissue culture chamber room under a 16-hour-light/8-hour-dark photoperiod at 21°C, except for the experiments done to reveal the pure *c*-CA and/or *t*-CA effect. Seedlings grown in darkness received a short 4h red light-pulse to induce germination. Propidium-iodide (PI; Sigma Aldrich) was used to counterstain the cell wall. The adventitious rooting assay was performed by placing plates in darkness for seven days (after a short light-pulse with red light of 4 hours). Plates were then exposed to light for 5 days. The root bending assay was performed on 5 days-old seedlings treated with different concentrations of *c/t*-CA. After 5 days plates were rotated 90 degrees and root gravitropism was scored after 48 hours. Scans were made and the quantification of the response was performed with ImageJ. Tobacco cells (*Nicotiana tabacum* L., cv Bright Yellow-2) of the cell line BY-2 (Nagata et al., 1992) were cultivated according to (Petrasek et al., 2006) and subcultured weekly. Bromophenol blue was used to stain the cell wall of *Physcomitrella patens* leaves.

Description of plant phenotype

To quantify growth parameters and check for aberrant phenotypes, seeds were grown on square plates placed in a vertical orientation in the growth chamber. Plates were scanned using the Scanmaker 9800XL and root length was measured using the ImageJ software. For

each compound, the inhibitory concentration (IC_{50}) was calculated, plotting a dose-response curve in SigmaPlot. The dose-response curve resulting in the highest R^2-value (coefficient of determination) was used. The number of plants used and the timing of the scanning depends on the plant species and the treatment. The number of adventitious roots (above the root-shoot junction) and number of emerged lateral roots were counted using a stereomicroscope (CETI Binocular Zoom Stereo).

Histochemical analysis and confocal microscopy

Root cell walls were stained with 30 µM PI for *pKNOLLE:KNOLLE-GFP* at the onset of the experiment. The excitation energy of 488 nm was from an argon laser. The PI fluorescence emission was collected between 550 and 650 nm, GFP/YFP between 500 and 550 nm. All images were captured with an inverted LSM 710 META confocal microscope equipped with 20x-Air objectives (Carl Zeiss, Jena, Germany). GUS-assays were performed and inspected using differential interference contrast optics as described earlier in Beeckman and Engler (Beeckman and Engler, 1994)

Time-lapse DII-VENUS

For analysis of chemically treated roots, seven days-old DII-VENUS Arabidopsis seedlings were transferred to 0.5xMS-media containing chemicals at the stated concentration. At the onset of the time-lapse, 3 seedlings (biological repeats) were placed in glass-bottomed dishes and covered with 0.5xMS-media containing NAA, NPA, *c*-CA or *t*-CA. The time-lapse was started 5 min after the seedlings had been placed in contact with the media and captured over 45 min (every 5 min) with an inverted LSM 710 META confocal microscope equipped with 20x-Air objectives (Carl Zeiss, Jena, Germany). Images were analyzed with the Fiji software using the total signal from Z-projection of defined region (always the same area). Normalization was done by using the initial signal from the Z-projection of adefined region as the baseline.

Time-lapse *DR5rev:GFP*

Seven days-old Arabidopsis seedlings were used to analyze the effect of *c*-CA, *t*-CA, NPA and NAA on the expression of DR5rev:GFP in the region between two emerged lateral roots. At the start of the time-lapse, seedlings were placed in glass-bottomed dishes and covered with media containing NAA, *c*-CA or *t*-CA. The time-lapse was started 5 min after the seedlings had been placed in contact with the media and captured over a period of 16h, every hour with an inverted LSM 710 META confocal microscope (Carl Zeiss, Jena, Germany) equipped with 20-Air objectives (Carl Zeiss, Jena, Germany). Images were analyzed with the Volocity software. The accumulation projection spectrum was obtained by

projecting the GFP intensity on a virtual line crossing the middle of the primary root over the imaged distance of the root. This way *DR5rev:GFP* expression can be imaged and quantified in every cell type. Normalization was performed against the intensity to the highest obtained signal at the earliest timepoint.

Time-lapse *DR5:LUC*

The *DR5:LUC* images were taken by a Lumazone machine carrying a charge-coupled device (CCD) camera (Princeton Instruments, Trenton, NJ, USA). The CCD camera that is controlled by a WinView/32 software took movies of the *DR5:LUC* expression automatically every 10 minutes (exposure time, 10 minutes) for 12 hours. Before imaging, plates containing 0.5xMS-medium were sprayed with 1 mM D-luciferin solution (Duchefa Biochemie). The picture series were saved as TIFF format for further analysis. The luciferase signals were quantified by the measure of the analog-digital units (ADU) per pixel by means of ImageJ. To visualize the spatiotemporal *DR5:LUC* signal changes during treatment with the compound, a Kymograph (http://www.embl.de/eamnet/html/body_kymograph.html) was generated with ImageJ.

Heterologous expression of C4H and microsome assay

The *Saccharomyces cerevisiae* strain containing the Arabidopsis *C4H* was used (Van de Wouwer et al., 2016). 100 µL of recombinant yeast in glycerol was grown overnight at 30°C in 5 mL liquid DO medium (Clontech Laboratories Inc., Mountain View, CA, USA). The yeast cells were pelleted (1 min at 4000 rpm), washed with 5 mL sterile MQ water, pelleted again, and resuspended in another 5 mL water. The amount of inoculum was calculated to reach an OD600 of 0.1 and subsequently, the yeast cultures were grown for 16h at 30°C with shaking (200 rpm) in DO medium (Clontech Laboratories Inc., Mountain View, CA, USA) containing galactose to induce transcription. Microsomes were prepared according to (Schalk et al., 1998). The microsome assay was done with aliquots of 10 µL microsome, by adding 20 mM sodium-phosphate-buffer (pH 7.4) (PBS), 10 µL of the desired compound at final concentrations of 10 µM for *c*-CA and *t*-CA and equal amounts of DMSO as a control. To start the reaction, 10 µL of the 10 mM $NADP^+$ PBS-solution was added to the Eppendorf, briefly vortexed and immediately placed in the Eppendorf thermomixer at 28 °C for 20 minutes. The reaction was stopped by adding 150 µL ice cold methanol. The pellet was resuspended in 500 µL 90% methanol and incubated in an Eppendorf thermomixer at 30°C for 10 min while shaking at 1000 rpm. After centrifugation at 14 000 rpm for 5 min, the supernatant was transferred to a new Eppendorf tube and lyophilized. The pellet was treated with 100 µL water and 100 µL cyclohexane. After 10 min of centrifugation (14 000 rpm), 80 µL of the aqueous phase was retained for UPLC-MS analysis. For reversed-phase LC, 10 µL

of the aqueous phase was subjected to UPLC-MS on a Waters Acquity system (Waters Corp., Milford, MA, USA) connected to a Thermo LTQ XL mass spectrometer (Thermo Scientific, Waltham, MA, USA). Chromatographic gradient separation was carried out as described in the next paragraph. The eluent was directed to the mass spectrometer via electrospray ionization (ESI) in negative mode. MS source parameters were as follows: capillary temperature, 300°C; capillary voltage, 24 V; source voltage, 3.5 V; source current, 100 A; sheath gas flow, 30; aux gas flow, 20; sweep gas flow, 5. The mass range was set between 100 and 1000 Da. *c*-CA, *t*-CA and *p*-coumaric acid were characterized based on the similarity of their masses and retention times with those of standards. Peak detection and integration was done with Progenesis QI v2.1 (Nonlinear Dynamics, a Waters Company, Newcastle, UK). Product/substrate ratios were calculated and p-values were calculated using Unpaired Student T-Tests.

Liquid chromatography-tandem mass spectrometry (LC-UV-Vis-MS) to determine *c*- and *t*-CA photo-isomerization

Exactly 2.5 mg of pure *t*-CA and *c*-CA was dissolved in 50.0 ml Milli-Q-H_2O/DMSO (80/20). Solutions were subsequently incubated in the growth chamber and isomerization of both isomers was followed over time by liquid chromatography-tandem mass spectrometry (LC-MS/MS). For darkness, plates were covered with aluminum foil, to exclude light and sampling was performed in darkness. Deep-red and far-red illumination was provided by the GreenPower LED module, Philips.

For quantification of *t*-CA and *c*-CA a 15 µl aliquot was subjected to LC-MS analysis performed on a Waters Acquity UPLC system equipped with a PDA detector (lambda range from 190 to 500 nm) (Waters Corp., Milford, MA, USA) connected to a Synapt HDMS quadrupole time-of-flight (Q-TOF) mass spectrometer (Waters MS Technologies, Manchester, UK). Chromatographic separation was performed on an Acquity UPLC BEH C18 column (2.1 mm × 150 mm, 1.7 µm; Waters Corp.) using a water-acetonitrile gradient elution. Mobile phases were composed of (A) water containing 1% acetonitrile (ACN) and 0.1% formic acid and (B) ACN containing 1% water and 0.1% formic acid. The column temperature was maintained at 40 °C, and the autosampler temperature was maintained at 10 °C. A flow rate of 350 µL/min was applied during the gradient elution, with initialization at time 0 min 5% (B), 30 min 50% (B), and 33 min 100% (B). For UV-Vis detection, data was recorded between 210 and 500 nm. The eluant was then directed to the mass spectrometer equipped with an electrospray ionization source and lockspray interface for accurate mass measurements. The MS source parameters were as follows: capillary voltage, 2.5 kV; sampling cone, 37 V; extraction cone, 3.5 V; source temperature, 120°C; desolvation temperature, 400°C; cone gas flow, 50 L h^{-1}; and desolvation gas flow, 550 L h^{-1}. The

collision energy for the trap and transfer cells was 6 and 4 V, respectively. For data acquisition, the dynamic range enhancement mode was activated. Full-scan data were recorded in negative centroid V-mode; the mass range between m/z 100 and 1000, with a scan speed of 0.2 s scan^{-1}. Leucin-enkephalin (250 pg µL^{-1}; solubilized in water: acetonitrile 1:1 [v/v] with 0.1% [v/v] formic acid) was used for lock mass calibration, with scanning every 10 s with a scan time of 0.5 s. All data was recorded with Masslynx software (version 4.1, Waters). For the quantification of *t*-CA and *c*-CA, the UV-Vis chromatogram was extracted at 277nm, and peaks were integrated automatically (automatic noise measurement; mean smoothing (window size: 3, number of smooths: 2)). Peak areas were used to calculate the conversion of *t*-CA and *c*-CA.

Auxin metabolite profiling

Extraction and purification of auxin and its metabolites was done as described previously with minor modifications (Novak et al., 2012). Frozen samples were homogenized using a MixerMill (Retsch GmbH, Haan, Germany) and extracted in 1 mL 50 mM sodium phosphate buffer (pH 7.0) containing antioxidant (1% sodium diethyldithiocarbamate) and a cocktail of deuterium and $^{13}C_6$-labeled internal standards of IAA and its metabolites. The pH was adjusted to 2.7 with 1 M hydrochloric acid, and the extracts were purified on Oasis HLB columns (30 mg, Waters Corp., Milford, USA), conditioned with 1 mL methanol, 1 mL water, and 0.5 mL sodium phosphate buffer (pH 2.7). After sample application, the column was washed with 2 mL 5% methanol and then eluted with 2 mL 80% methanol. Eluates were evaporated to dryness and dissolved in 20 µL of mobile phase prior to mass analysis using a 1290 Infinity LC system and 6460 Triple Quad LC/MS system (Agilent Technologies, Santa Clara, USA) (Novak et al., 2012).

Auxin accumulation assays

Assays were performed according to Petrášek *et al.* (Petrasek et al., 2003). Auxin accumulation was measured in tobacco BY-2 cells (*Nicotiana tabacum* L. cv. Bright Yellow 2; Nagata et al., 1992) 48 hours after subcultivation in 0.5 mL aliquots of cell suspension (target working cell density was 7×10^5 cells×mL^{-1}, and it was determined precisely by counting in the Fuchs-Rosenthal haemocytometer). Cultivation medium was removed by filtration on 20 µm mesh nylon filters and cells were resuspended in uptake buffer (20 mM MES, 10 mM sucrose, 0.5 mM $CaSO_4$, pH adjusted to 5.7 with KOH) and equilibrated for 45 minutes on the orbital shaker at 27 °C in darkness. Equilibrated cells were collected by filtration, resuspended in fresh uptake buffer and incubated with continuous orbital shaking for another 90 minutes under the same conditions. Radiolabelled auxin ([^{3}H]-naphthalene-1-acetic acid ([^{3}H]-NAA) or [^{3}H]-2,4-dichlorophenoxyacetic acid ([^{3}H]-2,4-D); specific (molar) radioactivity

20 Ci/mmol each; American Radiolabeled Chemicals, ARC Inc., St. Louis, MO, USA) was added to the cell suspension to a final concentration of 2 nM. At certain time points, aliquots of the cell suspension were sampled and accumulation of radiolabelled auxins was terminated by rapid filtration under reduced pressure on cellulose filters (22 mm in diameter). Cell cakes with filters were transferred into scintillation vials, extracted with ethanol (UV-spectroscopy grade) for 30 minutes and radioactivity was determined by liquid scintillation counting (Packard Tri-Carb 2900TR scintillation counter, Packard Instrument Co., Meridien, CT, USA). Counting efficiency was determined by automatic external standardization and counts were corrected for quenching automatically. For remaining surface radioactivity, counts were corrected by subtracting counts of aliquots collected immediately after addition of radiolabelled auxin. Inhibitors were added as required from stock solutions to an appropriate final concentration and proper controls (solvent) were applied. Recorded accumulation values were recalculated to 1 million cells.

Rootward auxin transport assays

Rootward auxin transport assays were performed as described previously (Geisler et al., 2005). Briefly, 0.1 µL microdroplets containing 500 nM [^{3}H]-IAA (American Radiolabelled Chemicals) and 500 nM cold' IAA (Sigma Aldrich) were placed on the shoot apical meristem of Arabidopsis seedlings and rootward auxin transport was measured by harvesting a 4 mm segment centered on the root shoot transition zone, as well as the entire root, in 2 mm segments (beginning with root zone-1 (RZ-1) just after the transition zone (TZ), and ending with the main root tip). Treatments with MS-media and 10 µM *c*-CA were carried out by saturating the filter paper matrix on which the roots were incubated during auxin transport assays with MS media supplemented with either a water:methanol blank or *c*-CA.

Auxin-binding and anti-auxin experiments using Surface Plasmon Resonance (SPR) and docking

Auxin receptor proteins AtTIR1 and AtAFB5 were expressed in insect cells (T. ni High5) and purified as described previously (Villalobos et al., 2012; Lee et al., 2014). The biotinylated degron peptide representing Aux/IAA7 was purchased from ThermoFisher Scientific (Loughborough, UK) and immobilized on streptavidin-coated SPR chips (GE Healthcare, Amersham, UK). SPR experiments were run as described previously (Villalobos et al., 2012; Lee et al., 2014). Briefly, compounds were added to purified receptor proteins from stock solutions in DMSO to give working concentrations which were 50 µM unless stated otherwise (DMSO 0.1% final). Controls lacking auxin/compound and controls containing IAA (50 µM) were run as references at the start and end of every set of sensorgrams on every protein preparation. Compounds were run in three separate

762 experiments, with characteristic results shown. For anti-auxin runs, receptor proteins were
763 mixed with 5 μM IAA plus compound at 50 μM. An anti-auxin effect was then determined if
764 the compound competed with IAA, reducing the amplitude of TIR1/AFB5 binding on the
765 sensorgram. Docking was performed using the Vina docking algorithm (Morris et al., 2009;
766 Trott and Olson, 2010). With the TIR1 crystal structure (PDB code 2P1P) from (Tan et al.,
767 2007). In-silico modeling, molecular graphics and analyses were performed with the UCSF
768 Chimera package. Chimera is open source and developed by the Resource for
769 Biocomputing, Visualization, and Informatics at the University of California, San Francisco
770 (supported by NIGMS P41-GM103311) (Pettersen et al., 2004). Marvin was used for
771 drawing, displaying and characterizing chemical structures, substructures and reactions.
772 Calculator Plugins were used for structure property prediction and calculation
773 Marvin v15.10.12.0, 2015, ChemAxon (http://www.chemaxon.com).
774

ACKNOWLEDGMENTS

We would like to thank Ottoline Leyser (Sainsbury Laboratory, University of Cambridge, Cambridge CB2 1LR) for providing us *p35S:iaaL* Arabidopsis seeds. We would Karel Spruyt imaging wherever needed, Toon Babylon for technical assistance, Wei Xua and Davy Opdenacker for help with the *DR5:LUC* experiments and Tao Fang and Hans Motte for providing us with the *Selaginella helvetica* plantlets.. We also appreciated the help of the VIB Imaging Core facility, namely Amanda Gonçalves, who helped analyzing the imaging experiments and Dominic Petrella for critical reading of the manuscript. Finally, we would like to thank Wim Grunewald, Tom Beeckman, Steffen Vanneste, Bert De Rybel and Jürgen Kleine-Vehn for scientific discussions.

TABLES

none

FIGURE LEGENDS

Figure 1. Effect of *c/t*-CA on growth and development of Arabidopsis.

(A) Root/rosette phenotype of representative seedlings 12 DAG, grown on 0.5xMS-medium supplemented with *c/t*-CA (n>20 for each concentration) (scale bar: 1 cm). (B) *c/t*-CA dose response curve for primary root growth (Sigmoidal-logistic, 4 parameters) (n>20). Error bars represent standard deviations. (C) Lateral root density of seedlings 12 DAG, grown on 0.5xMS-medium supplemented with *c/t*-CA (n>15). Error bars represent standard deviations and asterisks were used to indicate statistically significant differences compared to the corresponding mock-treated control sample as determined by Dunnett's test P-values: *P < 0.05, **P < 0.001, *** P <0.0001. (D) Representative light microscopic images of a root segment with lateral root primordia visualized by CYCB1:GUS expression in Arabidopsis 12 DAG of seedlings grown on 0.5xMS-medium supplemented with different concentrations of *c/t*-CA (n>10) (scale bar: 0.5 cm). (E) Number of adventitious roots of seedlings 12 DAG grown on 0.5xMS-medium supplemented with *c/t*-CA. Plants were grown for 7 days in darkness (after a short light-pulse of 4h with red-light to induce germination) and subsequently transferred to light to stimulate adventitious rooting. Adventitious root numbers are represented in grey-scale (n>20). (F-G) Binocular microscopic images of a root segment of the (F) primary root and (G) lateral root of seedlings 12 DAG, grown on 0.5xMS-medium

whether or not supplemented with 10 µM *c/t*-CA (n=10). (H) Histogram showing the *c/t*-CA-induced disruption of the gravitropic response in the main root. Seeds were germinated on 0.5xMS-medium and 4 DAG seedlings were transferred to 0.5xMS-medium supplemented with c/t-CA. Subsequently, seedlings growing on vertical plates were rotated 90 degrees and each root was assigned to one of 12 30° sectors after 48h incubation (n>25).

Figure 2. Effect of *c*-CA on root architecture.

Dose response curves (Sigmoidal-logistic, 4 parameters) showing the effect of *c*-CA (triangles) or *t*-CA (dots) on (A) hypocotyl and (B) root length of seedlings 12 DAG, grown in darkness on 0.5xMS-medium supplemented with either *c*- or *t*-CA (n>20). Seed germination was induced by a 4h red light-pulse. (C) Confocal images showing KNOLLE promoter activity (green) of 10 DAG pKNOLLE:KNOLLE-GFP seedlings. (D-E) Light microscopic images of *c*-CA induced GUS activity in 10 DAG pPGAZAT:GUS and pGATA23:GUS seedlings. GUS activity was monitored at the lateral roots (PGAZAT) or the zone basal to the main root tip (GATA23). For the GATA23 driven GUS expression the main root tip is shown as inset. For (C) and (D), seeds were germinated on 0.5xMS-medium and 7 DAG seedlings were transferred to 0.5xMS-medium supplemented with 10 µM *c*-CA or *t*-CA (n=5) (scale bar: 15 µm).Growth conditions for (E) were as for (C) with the only exception that *c*-CA and *t*-CA were used at 2.5 µM (n=5).

Figure 3. *c*-CA induces an auxin response in Arabidopsis.

(A) Kymograph of pDR5:LUC intensity along the primary root of Arabidopsis seedlings during a 12h period. The kymograph represents on the vertical axis the primary root, with the root tip present in the orignin of the coordinate system, and the shoot/root junction at the end of the vertical axis. The horizontal axis represents time. Seeds were germinated on 0.5xMS-medium and 5 DAG seedlings were transferred to 0.5xMS-medium supplemented with 1-10 µM *c*-CA, 10 µM *t*-CA or 1 µM NAA. Imaging was started at the moment of transfer and data was recorded every 10 minutes. Each kymograph represents one experiment. The kymograph is representative for 8 biological repeats (seedlings). B) Confocal time-lapse imaging of pDR5rev:GFP intensity in the primary root between two young emerged lateral roots. At the start of the time-lapse, seedlings were placed in glass-bottomed dishes and covered with 0.5xMS-medium containing 1 µM NAA, 1-10 µM *c*-CA or 10 µM *t*-CA. The time-lapse was started 5 minutes after the seedlings had been placed in contact with the media

and captured every 60 minutes over a 16h period. Cumulative spectra were obtained by projecting the GFP intensity on a virtual line crossing the middle of the primary root. Normalization was performed against the maximal intensity of the signal at the earliest time point (n=1). Each spectrum is representative for 3 biological repeats (positions along the primary root).

Figure 4. *c*-CA does not act as a typical auxin.

(A) Root phenotype of arf7 arf19, slr and tir1 afb2 afb3 mutants 12 DAG, growing on 0.5xMS medium supplemented with 10 µM *c/t*-CA (n>25) (scale bar: 1 cm). (B) Surface Plasmon Resonance sensorgrams showing the auxin-depended interaction between TIR1 or AFB5 with IAA DII. Each sensorgram shows the binding with IAA (blue), an auxin-free injection (red) plus the data for each test compound (green). For auxin activity assays (top) compounds (50 µM) were mixed with TIR1 or AFB5 prior to injection over DII peptide. For anti-auxin assays (bottom), compounds (50 µM) were mixed with TIR1 or AFB5 plus 5 µM IAA prior to injection. The degron sequence that was used: biot-AKAQVVGWPPVRNYRKN.

Figure 5. Effect of *c*-CA on polar auxin transport.

(A) Time-course of DII-VENUS fluorescence in the main root tip of DII-VENUS-YFP seedlings. Plants were germinated on 0.5xMS-medium and subsequently transferred 5 DAG to 0.5xMS-medium supplemented with 1 or 10 µM *c*-CA, 10 µM *t*-CA or 1 µM 1-NAA (n=3). (scale bar: 50 µm). Fluorescence was quantified every 3 minutes over a 42 minute period. During each experiment 3 root tips (representing one treatment) were simultaneously imaged. Error bars represent standard deviations. (B) Effect of 10 µM *c*-CA, *t*-CA or NPA on the net accumulation of [3H]-NAA in 2-day old suspension-cultured tobacco BY-2 cells (20 minute uptake period). The arrows points to the time of application of the compound. Error bars represent standard deviations (n=4). (C) Model explaining the *c*-CA mediated lateral root proliferation. *c*-CA inhibits shootward auxin transport by inhibiting the redistribution of auxin in the meristem. This is considered a direct consequence of the *c*-CA mediated inhibition of auxin efflux. The phloem-mediated rootward auxin transport in the primary root is not disturbed by *c*-CA, allowing a continuos supply of auxin from the shoot towards the root tip. The block of a proper auxin redistribution in the meristem results in the accumulation of auxin in the primary root, where it triggers lateral root proliferation. Top: auxin flow (blue arrows) and its perturbation within the primary root of *c*-CA treated plants. Bottom: schematic

887 represenatiation of auxin accumulation in the primary root of *c*-CA treated plants and the
888 consequent induction of lateral roots.
889
890
891 **SUPPLEMENTAL FIGURES**
892
893 **Figure S1.** The general phenylpropanoid pathway.
894 **Figure S2.** Effect of *c*/*t*-CA on growth and development of different plant species.
895 **Figure S3.** Photo-isomerization of *c*-CA and *t*-CA.
896 **Figure S4.** Conversion of *t*-CA by C4H in Arabidopsis.
897 **Figure S5.** Effect of *c*-CA on GATA23 expression.
898 **Figure S6.** Time dependent *DR5* driven *LUC* expression upon *c*-CA treatment.
899 **Figure S7.** Time dependent *DR5* driven *GFP* expression upon *c*-CA treatment.
900 **Figure S8.** Docking of *c*-CA and *t*-CA to the auxin binding pocket of TIR1.
901 **Figure S9**. Shift in IAA related metabolites upon treatment with 10 µM *c*-CA and *t*-CA for 1h.
902 **Figure S10**. Shift in the IAA metabolome upon treatment with 10 µM *c*-CA and *t*-CA for 6h.
903 **Figure S11.** The effect on IAA reduction on *c*-CA mediated developmental defects in
904 seedlings.
905 **Figure S12.** DII-VENUS response to *c*-CA.
906 **Figure S13.** DII-VENUS response to NPA.
907 **Figure S14.** The effect of combined treatment with *c*-CA and NPA on auxin accumulation.
908 **Figure S15.** The effect of combined treatment with *c*-CA and BUM on auxin accumulation.
909 **Figure S16.** The effect of *c*-CA on polar auxin transport.
910 **Figure S17.** Time dependent *DR5* driven *LUC* expression upon local application of
911 *c*-CA.
912 **Figure S18.** The effect of *c*-CA on long distance rootward auxin transport in Arabidopsis.
913
914

915

916

Parsed Citations

Åberg B (1961) Studies on plant growth regulator XVIII. Some ß-substituted acrylic acids. Kungliga lantbrukshogskolans 27: 99-123
Pubmed: Author and Title
CrossRef: Author and Title
Google Scholar: Author Only Title Only Author and Title

Adamowski M, Friml J (2015) PIN-Dependent Auxin Transport: Action, Regulation, and Evolution. Plant Cell 27: 20-32
Pubmed: Author and Title
CrossRef: Author and Title
Google Scholar: Author Only Title Only Author and Title

Beeckman T, Engler G (1994) An easy technique for the clearing of histochemically stained plant tissue. Plant Molecular Biology Reporter 12: 37-42
Pubmed: Author and Title
CrossRef: Author and Title
Google Scholar: Author Only Title Only Author and Title

Benkova E, Michniewicz M, Sauer M, Teichmann T, Seifertova D, Jurgens G, Friml J (2003) Local, efflux-dependent auxin gradients as a common module for plant organ formation. Cell 115: 591-602
Pubmed: Author and Title
CrossRef: Author and Title
Google Scholar: Author Only Title Only Author and Title

Boerjan W, Ralph J, Baucher M (2003) Lignin biosynthesis. Annual Review of Plant Biology 54: 519-546
Pubmed: Author and Title
CrossRef: Author and Title
Google Scholar: Author Only Title Only Author and Title

Brown DE, Rashotte AM, Murphy AS, Normanly J, Tague BW, Peer WA, Taiz L, Muday GK (2001) Flavonoids act as negative regulators of auxin transport in vivo in Arabidopsis. Plant Physiology 126: 524-535
Pubmed: Author and Title
CrossRef: Author and Title
Google Scholar: Author Only Title Only Author and Title

Brunoud G, Wells DM, Oliva M, Larrieu A, Mirabet V, Burrow AH, Beeckman T, Kepinski S, Traas J, Bennett MJ, Vernoux T (2012) A novel sensor to map auxin response and distribution at high spatio-temporal resolution. Nature 482: 103-106
Pubmed: Author and Title
CrossRef: Author and Title
Google Scholar: Author Only Title Only Author and Title

Buer CS, Kordbacheh F, Truong TT, Hocart CH, Djordjevic MA (2013) Alteration of flavonoid accumulation patterns in transparent testa mutants disturbs auxin transport, gravity responses, and imparts long-term effects on root and shoot architecture. Planta 238: 171-189
Pubmed: Author and Title
CrossRef: Author and Title
Google Scholar: Author Only Title Only Author and Title

Colon-Carmona A, You R, Haimovitch-Gal T, Doerner P (1999) Spatio-temporal analysis of mitotic activity with a labile cyclin-GUS fusion protein. Plant Journal 20: 503-508
Pubmed: Author and Title
CrossRef: Author and Title
Google Scholar: Author Only Title Only Author and Title

De Rybel B, Vassileva V, Parizot B, Demeulenaere M, Grunewald W, Audenaert D, Van Campenhout J, Overvoorde P, Jansen L, Vanneste S, Moller B, Wilson M, Holman T, Van Isterdael G, Brunoud G, Vuylsteke M, Vernoux T, De Veylder L, Inze D, Weijers D, Bennett MJ, Beeckman T (2010) A Novel Aux/IAA28 Signaling Cascade Activates GATA23-Dependent Specification of Lateral Root Founder Cell Identity. Current Biology 20: 1697-1706
Pubmed: Author and Title
CrossRef: Author and Title
Google Scholar: Author Only Title Only Author and Title

Delbarre A, Muller P, Imhoff V, Guern J (1996) Comparison of mechanisms controlling uptake and accumulation of 2,4-dichlorophenoxy acetic acid, naphthalene-1-acetic acid, and indole-3-acetic acid in suspension-cultured tobacco cells. Planta 198: 532-541
Pubmed: Author and Title
CrossRef: Author and Title
Google Scholar: Author Only Title Only Author and Title

Dharmasiri N, Dharmasiri S, Weijers D, Lechner E, Yamada M, Hobbie L, Ehrismann JS, Jurgens G, Estelle M (2005) Plant development is regulated by a family of auxin receptor F box proteins. Developmental Cell 9: 109-119
Pubmed: Author and Title
CrossRef: Author and Title
Google Scholar: Author Only Title Only Author and Title

Ding ZJ, Galvan-Ampudia CS, Demarsy E, Langowski L, Kleine-Vehn J, Fan YW, Morita MT, Tasaka M, Fankhauser C, Offringa R, Friml J (2011) Light-mediated polarization of the PIN3 auxin transporter for the phototropic response in Arabidopsis. Nature Cell Biology 13: 447-453
Pubmed: Author and Title

CrossRef: Author and Title
Google Scholar: Author Only Title Only Author and Title

Friml J, Vieten A, Sauer M, Weijers D, Schwarz H, Hamann T, Offringa R, Jurgens G (2003) Efflux-dependent auxin gradients establish the apical-basal axis of Arabidopsis. Nature 426: 147-153
Pubmed: Author and Title
CrossRef: Author and Title
Google Scholar: Author Only Title Only Author and Title

Fukaki H, Tameda S, Masuda H, Tasaka M (2002) Lateral root formation is blocked by a gain-of-function mutation in the SOLITARY-ROOT/IAA14 gene of Arabidopsis. Plant Journal 29: 153-168
Pubmed: Author and Title
CrossRef: Author and Title
Google Scholar: Author Only Title Only Author and Title

Gonzalez-Carranza ZH, Elliott KA, Roberts JA (2007) Expression of polygalacturonases and evidence to support their role during cell separation processes in Arabidopsis thaliana. J Exp Bot 58: 3719-3730
Pubmed: Author and Title
CrossRef: Author and Title
Google Scholar: Author Only Title Only Author and Title

Haagen-Smit SAJW, F.W. (1935) A physiological analysis of the growth substance. Proceedings, Koninklijke Akademie van Wetenschappen te Amsterdam 38: 852-857
Pubmed: Author and Title
CrossRef: Author and Title
Google Scholar: Author Only Title Only Author and Title

Hitchcock AE (1935) Indole-3-n-propionic acid as a growth hormone and quantitative measurement of plant response. Contributions from Boyce Thompson Institute 7: 87-95
Pubmed: Author and Title
CrossRef: Author and Title
Google Scholar: Author Only Title Only Author and Title

Hoyerova K, Hosek P, Kubes M, Lankova M, Kohoutova M, Dobrev PI, Jirina M, Petrasek J, Zazimalova E (2011) Auxin transport on cellular level by means of mathematical-modelling-motivated research. Febs Journal 278: 314-314
Pubmed: Author and Title
CrossRef: Author and Title
Google Scholar: Author Only Title Only Author and Title

Kim JY, Henrichs S, Bailly A, Vincenzetti V, Sovero V, Mancuso S, Pollmann S, Kim D, Geisler M, Nam HG (2010) Identification of an ABCB/P-glycoprotein-specific Inhibitor of Auxin Transport by Chemical Genomics. Journal of Biological Chemistry 285: 23307-23315
Pubmed: Author and Title
CrossRef: Author and Title
Google Scholar: Author Only Title Only Author and Title

Koepfli JB, Thimann KB, Went FW (1938) Plant hormones: structure and physiological activity. Journal of Biological Chemistry 122: 763-780
Pubmed: Author and Title
CrossRef: Author and Title
Google Scholar: Author Only Title Only Author and Title

Kumpf RP, Shi CL, Larrieu A, Sto IM, Butenko MA, Peret B, Riiser ES, Bennett MJ, Aalen RB (2013) Floral organ abscission peptide IDA and its HAE/HSL2 receptors control cell separation during lateral root emergence. Proc Natl Acad Sci U S A 110: 5235-5240
Pubmed: Author and Title
CrossRef: Author and Title
Google Scholar: Author Only Title Only Author and Title

Lee S, Sundaram S, Armitage L, Evans JP, Hawkes T, Kepinski S, Ferro N, Napier RM (2014) Defining Binding Efficiency and Specificity of Auxins for SCFTIR1/AFB-Aux/IAA Co-receptor Complex Formation. Acs Chemical Biology 9: 673-682
Pubmed: Author and Title
CrossRef: Author and Title
Google Scholar: Author Only Title Only Author and Title

Letham DS (1978) Natural-occurring plant growth regulations other than the principal hormones of higher plants. Phytohormones and Related Compounds - A Comprehensive Treatise 38: 85-92
Pubmed: Author and Title
CrossRef: Author and Title
Google Scholar: Author Only Title Only Author and Title

Liu CM, Xu ZH, Chua NH (1993) Auxin Polar Transport Is Essential for the Establishment of Bilateral Symmetry during Early Plant Embryogenesis. Plant Cell 5: 621-630
Pubmed: Author and Title
CrossRef: Author and Title
Google Scholar: Author Only Title Only Author and Title

Lukowitz W, Mayer U, Jurgens G (1996) Cytokinesis in the Arabidopsis embryo involves the syntaxin-related KNOLLE gene product. Cell 84: 61-71
Pubmed: Author and Title
CrossRef: Author and Title
Google Scholar: Author Only Title Only Author and Title

Moreno-Risueno MA, Van Norman JM, Moreno A, Zhang JY, Ahnert SE, Benfey PN (2010) Oscillating Gene Expression Determines Competence for Periodic Arabidopsis Root Branching. Science 329: 1306-1311
Pubmed: Author and Title
CrossRef: Author and Title
Google Scholar: Author Only Title Only Author and Title

Morris GM, Huey R, Lindstrom W, Sanner MF, Belew RK, Goodsell DS, Olson AJ (2009) AutoDock4 and AutoDockTools4: Automated Docking with Selective Receptor Flexibility. Journal of Computational Chemistry 30: 2785-2791
Pubmed: Author and Title
CrossRef: Author and Title
Google Scholar: Author Only Title Only Author and Title

Nagata T, Nemoto Y, Hasezawa S (1992) Tobacco by-2 Cell-Line as the Hela-Cell in the Cell Biology of Higher-Plants. International Review of Cytology-a Survey of Cell Biology 132: 1-30
Pubmed: Author and Title
CrossRef: Author and Title
Google Scholar: Author Only Title Only Author and Title

Novak O, Henykova E, Sairanen I, Kowalczyk M, Pospisil T, Ljung K (2012) Tissue-specific profiling of the Arabidopsis thaliana auxin metabolome. Plant Journal 72: 523-536
Pubmed: Author and Title
CrossRef: Author and Title
Google Scholar: Author Only Title Only Author and Title

Okushima Y, Fukaki H, Onoda M, Theologis A, Tasaka M (2007) ARF7 and ARF19 regulate lateral root formation via direct activation of LBD/ASL genes in Arabidopsis. Plant Cell 19: 118-130
Pubmed: Author and Title
CrossRef: Author and Title
Google Scholar: Author Only Title Only Author and Title

Peret B, De Rybel B, Casimiro I, Benkova E, Swarup R, Laplaze L, Beeckman T, Bennett MJ (2009) Arabidopsis lateral root development: an emerging story. Trends Plant Sci 14: 399-408
Pubmed: Author and Title
CrossRef: Author and Title
Google Scholar: Author Only Title Only Author and Title

Petrasek J, Cerna A, Schwarzerova K, Elckner M, Morris DA, Zazimalova E (2003) Do phytotropins inhibit auxin efflux by impairing vesicle traffic? Plant Physiology 131: 254-263
Pubmed: Author and Title
CrossRef: Author and Title
Google Scholar: Author Only Title Only Author and Title

Petrasek J, Mravec J, Bouchard R, Blakeslee JJ, Abas M, Seifertova D, Wisniewska J, Tadele Z, Kubes M, Covanova M, Dhonukshe P, Skupa P, Benkova E, Perry L, Krecek P, Lee OR, Fink GR, Geisler M, Murphy AS, Luschnig C, Zazimalova E, Friml J (2006) PIN proteins perform a rate-limiting function in cellular auxin efflux. Science 312: 914-918
Pubmed: Author and Title
CrossRef: Author and Title
Google Scholar: Author Only Title Only Author and Title

Pettersen EF, Goddard TD, Huang CC, Couch GS, Greenblatt DM, Meng EC, Ferrin TE (2004) UCSF chimera - A visualization system for exploratory research and analysis. Journal of Computational Chemistry 25: 1605-1612
Pubmed: Author and Title
CrossRef: Author and Title
Google Scholar: Author Only Title Only Author and Title

Romano CP, Hein MB, Klee HJ (1991) Inactivation of Auxin in Tobacco Transformed with the Indoleacetic-Acid Lysine Synthetase Gene of Pseudomonas-Savastanoi. Genes & Development 5: 438-446
Pubmed: Author and Title
CrossRef: Author and Title
Google Scholar: Author Only Title Only Author and Title

Santelia D, Henrichs S, Vincenzetti V, Sauer M, Bigler L, Klein M, Bailly A, Lee Y, Friml J, Geisler M, Martinoia E (2008) Flavonoids Redirect PIN-mediated Polar Auxin Fluxes during Root Gravitropic Responses. Journal of Biological Chemistry 283: 31218-31226
Pubmed: Author and Title
CrossRef: Author and Title
Google Scholar: Author Only Title Only Author and Title

Schalk M, Cabello-Hurtado F, Pierrel MA, Atanossova R, Saindrenan P, Werck-Reichhart D (1998) Piperonylic acid, a selective, mechanism-based inactivator of the trans-cinnamate 4-hydroxylase: A new tool to control the flux of metabolites in the phenylpropanoid pathway. Plant Physiology 118: 209-218
Pubmed: Author and Title
CrossRef: Author and Title
Google Scholar: Author Only Title Only Author and Title

Trott O, Olson AJ (2010) Software News and Update AutoDock Vina: Improving the Speed and Accuracy of Docking with a New Scoring Function, Efficient Optimization, and Multithreading. Journal of Computational Chemistry 31: 455-461
Pubmed: Author and Title
CrossRef: Author and Title
Google Scholar: Author Only Title Only Author and Title

Van Overbeek J, Blondeau R, Horne V (1951) Trans-cinnamic acid as an anti-auxin. American Journal of Botany 38: 589-595
Pubmed: Author and Title
CrossRef: Author and Title
Google Scholar: Author Only Title Only Author and Title

Vanneste S, Friml J (2009) Auxin: A Trigger for Change in Plant Development. Cell 136: 1005-1016
Pubmed: Author and Title
CrossRef: Author and Title
Google Scholar: Author Only Title Only Author and Title

Villalobos LIAC, Lee S, De Oliveira C, Ivetac A, Brandt W, Armitage L, Sheard LB, Tan X, Parry G, Mao HB, Zheng N, Napier R, Kepinski S, Estelle M (2012) A combinatorial TIR1/AFB-Aux/IAA co-receptor system for differential sensing of auxin. Nature Chemical Biology 8: 477-485
Pubmed: Author and Title
CrossRef: Author and Title
Google Scholar: Author Only Title Only Author and Title

Vogt T (2010) Phenylpropanoid Biosynthesis. Molecular Plant 3: 2-20
Pubmed: Author and Title
CrossRef: Author and Title
Google Scholar: Author Only Title Only Author and Title

Went FW (1939) Analysis and integration of various auxin effects. I and II. Proceedings, Koninklijke Akademie van Wetenschappen te Amsterdam XLII: 731-739
Pubmed: Author and Title
CrossRef: Author and Title
Google Scholar: Author Only Title Only Author and Title

Wong WS, Guo D, Wang XL, Yin ZQ, Xia B, Li N (2005) Study of cis-cinnamic acid in Arabidopsis thaliana. Plant Physiology and Biochemistry 43: 929-937
Pubmed: Author and Title
CrossRef: Author and Title
Google Scholar: Author Only Title Only Author and Title

Yang XX, Choi HW, Yang SF, Li N (1999) A UV-light activated cinnamic acid isomer regulates plant growth and gravitropism via an ethylene receptor-independent pathway. Aust J Plant Physiol 26: 325-335
Pubmed: Author and Title
CrossRef: Author and Title
Google Scholar: Author Only Title Only Author and Title

Yin RH, Han K, Heller W, Albert A, Dobrev PI, Zazimalova E, Schaffner AR (2014) Kaempferol 3-O-rhamnoside-7-O-rhamnoside is an endogenous flavonol inhibitor of polar auxin transport in Arabidopsis shoots. New Phytologist 201: 466-475
Pubmed: Author and Title
CrossRef: Author and Title
Google Scholar: Author Only Title Only Author and Title

Yin ZQ, Wong WS, Ye WC, Li N (2003) Biologically active cis-cinnamic acid occurs naturally in Brassica parachinensis. Chinese Science Bulletin 48: 555-558
Pubmed: Author and Title
CrossRef: Author and Title
Google Scholar: Author Only Title Only Author and Title